Journal of
Synchrotron
Radiation

ISSN 1600-5775

Received 29 July 2014
Accepted 14 November 2014

Extended X-ray absorption fine structure and multiple-scattering simulation of nickel dithiolene complexes $Ni[S_2C_2(CF_3)_2]_2^n$ (n = −2, −1, 0) and an olefin adduct $Ni[S_2C_2(CF_3)_2]_2$(1-hexene)

Weiwei Gu,[a,b]‡ Hongxin Wang[a,c]*‡ and Kun Wang[d]‡

[a]Physical Biosciences Division, Lawrence Berkeley National Laboratory, 1 Cyclotron Road, Berkeley, CA 94720, USA, [b]UC Berkeley Extension, 1995 University Avenue, Berkeley, CA 94704, USA, [c]Department of Chemistry, University of California, 1 Shields Avenue, Davis, CA 95616, USA, and [d]Corporate Strategic Research, ExxonMobil Research and Engineering Co, 1545 Rt 22 East, Annandale, NJ 08801, USA. *E-mail: hxwang2@lbl.gov

A series of Ni dithiolene complexes $Ni[S_2C_2(CF_3)]_2^n$ (n = −2, −1, 0) (**1**, **2**, **3**) and a 1-hexene adduct $Ni[S_2C_2(CF_3)_2]_2(C_6H_{12})$ (**4**) have been examined by Ni *K*-edge X-ray absorption near-edge structure (XANES) and extended X-ray absorption fine-structure (EXAFS) spectroscopies. Ni XANES for **1**–**3** reveals clear pre-edge features and approximately +0.7 eV shift in the Ni *K*-edge position for 'one-electron' oxidation. EXAFS simulation shows that the Ni—S bond distances for **1**, **2** and **3** (2.11–2.16 Å) are within the typical values for square planar complexes and decrease by ∼0.022 Å for each 'one-electron' oxidation. The changes in Ni *K*-edge energy positions and Ni—S distances are consistent with the 'non-innocent' character of the dithiolene ligand. The Ni—C interactions at ∼3.0 Å are analyzed and the multiple-scattering parameters are also determined, leading to a better simulation for the overall EXAFS spectra. The 1-hexene adduct **4** presents no pre-edge feature, and its Ni *K*-edge position shifts by −0.8 eV in comparison with its starting dithiolene complex **3**. Consistently, EXAFS also showed that the Ni—S distances in **4** elongate by ∼0.046 Å in comparison with **3**. The evidence confirms that the neutral complex is 'reduced' upon addition of olefin, presumably by olefin donating the π-electron density to the LUMO of **3** as suggested by UV/visible spectroscopy in the literature.

Keywords: Ni dithiolene complexes; olefin adduct; extended X-ray absorption fine structure (EXAFS); X-ray absorption near-edge structure (XANES); single scattering; multiple scattering.

1. Introduction

Metal dithiolene complexes have been studied extensively since the 1960s (McCleverty, 1968; Rehr *et al.*, 1991; Schrauzer, 1969). While initial interests focused primarily on their redox and electronic properties (Billig *et al.*, 1964; Davison & Holm, 1967; Olson *et al.*, 1966), later studies have been stimulated by their potential applications in areas encompassing photo-energy conversion (Paw *et al.*, 1998), non-linear optics (Chen *et al.*, 1998; Winter *et al.*, 1992), Q-switch laser dyes (Mueller-Westerhoff *et al.*, 1991) and light-driven information devices (Mueller-Westerhoff *et al.*, 1991). All of these applications are associated with the unique non-innocent nature of 1,2-dithiolene ligands {*e.g.* $[S_2C_2(CF_3)_2]^{2-}$}, *i.e.* the dithiolene ligand can participate in the redox process of the coordination complex rather than just a spectator (Gray, 1965; Gu *et al.*, 2014). Ni dithiolene complexes have also attracted extensive interest due to their relevance to Ni-containing enzymes (Reedijk & Bouwman, 1999; Yadav *et al.*, 1997), such as NiFe hydrogenase (NiFe H_2ase), carbon monoxide dehydrogenase (CODH) and acetyl-CoA synthetase.

Ni dithiolene complexes have also been found to react with olefins to form 1/1 olefin adducts, where the olefin binds to the S atoms across the ligands (Schrauzer & Mayweg, 1965; Wing & Schlupp, 1970). For example, the complex $Ni[S_2C_2(CF_2)_2]_2$ can react with light olefins, including 1-hexene (Fig. 1) (Harrison *et al.*, 2006). The olefin–nickel products are an important type of charge-transfer adducts, which are relevant to selective olefin separation and possibly olefin detection. The interaction was proposed as electrophilic addition of Ni

‡ All authors contributed equally.

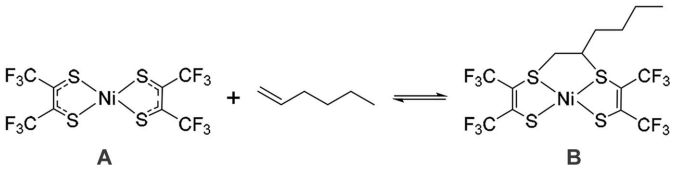

Figure 1
Formation of 1-hexene adduct with $Ni[S_2C_2(CF_2)_2]_2$ (**3**, **A**).

dithiolene (such as **A**) to the olefin to form an olefin adduct [such as **B** (Wang & Stiefel, 2001)]. The 744 nm band in the UV/visible absorption spectrum for **A**, which was assigned as the transition from the highest occupied molecular orbital (HOMO) to the lowest unoccupied molecular orbital (LUMO), disappeared partially in **B** (Wang & Stiefel, 2001), consistent with the olefin donating electron density to the LUMO of the dithiolene. However, optical transition is not element specific, thus the change of electron density in Ni cannot be probed specifically using UV/visible spectroscopy.

X-ray absorption spectroscopy (XAS) monitors the transition of a core electron to the valence shell, and is one of the most useful element-specific methods for studying metal centers in chemical complexes and metalloenzymes (Wang *et al.*, 2000). *K*-edge X-ray spectroscopy of Ni uses hard X-ray radiation and probes the transitions $1s \rightarrow$ pre-edge ($3d$ or $4p_z$ pre-edge features), $1s \rightarrow$ edge (X-ray absorption near-edge structure, XANES) and $1s \rightarrow$ continuum (extended X-ray absorption fine structure, EXAFS). EXAFS is the oscillating part from 100 eV to 1000 eV above the absorption edge. It is due to the interference between the outgoing photoelectron wave from metal and the electron wave in the ligand scatterers, and contains information about the chemical environment around the metal sites, such as type of ligands, coordination numbers and, most importantly, metal–ligand (M–L) distances.

Single scattering (SS) refers to the photoelectron wave scattering processes, in which one neighboring scatterer is involved in one scattering path, such as the first two cases in Fig. 2 (SS 1 and SS 2). In the case where two or more scattering atoms are involved in one scattering path (or one photoelectron wave source), it becomes multiple scattering (MS), as shown in Fig. 2 (MS A $\rightarrow$ MS G). It is clear that MS is dependent on both distance and angles of the scattering atoms and becomes a two-dimensional polar coordinate system. Each EXAFS spectrum will be the sum of SS and MS contributions, but the latter is usually weak and can be omitted in most cases. Nevertheless, the MS effect is a powerful tool to help determine geometric details, especially for highly symmetric complexes.

We recently reported Ni *L*-edge and *K*-edge X-ray absorption spectroscopy on the nickel oxidation state changes in a series of $Ni[S_2C_2(CF_3)_2]_2^n$ ($n = -2, -1, 0$) dithiolenes (Gu *et al.*, 2014). In this publication, we use Ni *K*-edge EXAFS to probe changes in the local molecular structure of the dithiolene complexes upon formal oxidation and olefin adduct formation. EXAFS spectra are analyzed with both SS and MS simulations, to obtain detailed Ni—S and Ni—C bond distances as well as the MS parameters for: $(Ph_4As)_2Ni[S_2C_2(CF_3)_2]_2$ (**1**) (Davison & Holm, 1967), $(^nBu_4N)Ni[S_2C_2(CF_3)_2]_2$ (**2**) (Davison & Holm, 1967) and $Ni[S_2C_2(CF_3)_2]_2$ (**3**) (Wang *et al.*, 2007). The Ni *K*-edge XANES and EXAFS for the 1-hexene adduct $Ni[S_2C_2(CF_3)_2]_2(C_6H_{12})$ (**4**) were also studied. This is a first XAS study on a dithiolene–olefin adduct. The bond distances from EXAFS are consistent with available crystallographic data (Penner-Hahn, 1999; Westre *et al.*, 1997; Wang *et al.*, 2007) for **2**, **3** and for the ethylene adduct $Ni[S_2C_2(CF_3)_2]_2(C_2H_4)$ (Harrison *et al.*, 2006) (which is similar to **4**). The differences in XANES and EXAFS among **1**, **2**, **3** and the 1-hexene adduct **4** are also discussed.

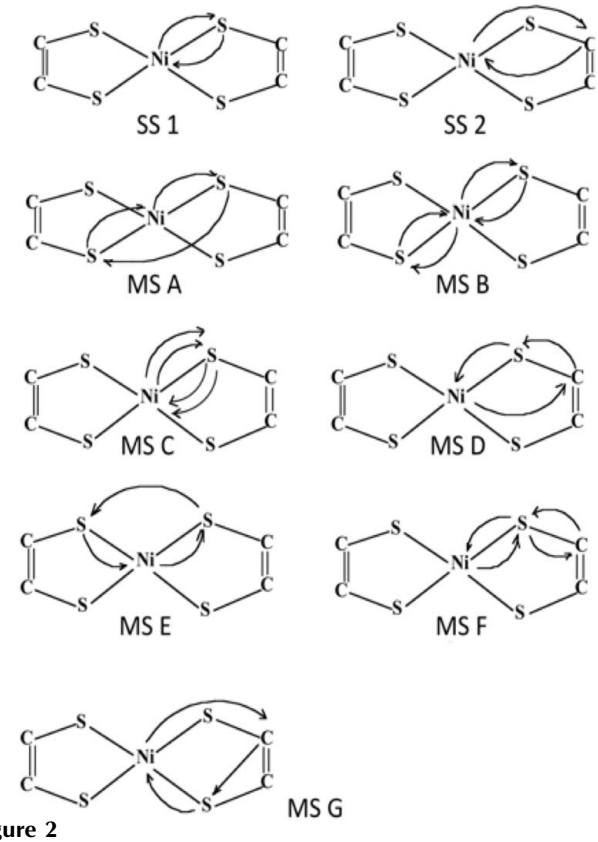

Figure 2
Single-scattering (SS) and multiple-scattering (MS) paths within Ni dithiolene calculated by *FEFF* 7.0.1.

2. Experimental procedures

2.1. Sample preparation

The nickel dithiolene complexes used in this study, $(Ph_4As)_2Ni[S_2C_2(CF_3)_2]_2$ (**1**) (Davison & Holm, 1967), $(^nBu_4N)Ni[S_2C_2(CF_3)_2]_2$ (**2**) (Davison & Holm, 1967), $Ni[S_2C_2(CF_3)_2]_2$ (**3**) (Wang *et al.*, 2007) and the olefin adducted $Ni[S_2C_2(CF_3)_2]_2(C_6H_{12})$ (**4**) (Wang & Stiefel, 2001), were synthesized following literature methods. The powdered solid samples were handled under nitrogen atmosphere (inside a glovebox) prior to the *K*-edge XANES and EXAFS measurements, although the measurements were performed under ambient conditions. The solid samples were ground and

mixed with boron nitride to dilute each sample to the proper Ni concentration, allowing it to have one X-ray optical density (for obtaining the best signal-to-noise ratio). The energy calibration sample (Ni foil) was purchased from Sigma-Aldrich and used as purchased (purity = 99.5%).

2.2. Measurements and analysis

Ni *K*-edge XAS data for Ni dithiolenes **1**, **2**, **3** and **4** were collected at beamline 2-3 at the Stanford Synchrotron Radiation Laboratory (SSRL). Si(111) monochromator crystals were used with 2 mm slits for EXAFS scans and 1 mm slits for the XANES spectra. Harmonic rejection was accomplished by detuning the second monochromator crystal to the position that has a flux at 50% of its maximum value. Data were collected in transmission mode in a typical three ion-chamber geometry with Ni dithiolene sample between I_0 and I_1 and the Ni foil between I_1 and I_2. All ion-chambers were filled with N_2. The energy was calibrated by setting the first inflection point of the Ni foil spectrum to 8331.6 eV. Each final spectrum was the sum of three 20 min scans.

The extraction of EXAFS oscillations from the final spectra was accomplished using the *EXAFSPAK* analysis software (George, 2009). E_0 was chosen as 8350 eV for defining the photoelectron wavevector k. $\Delta E = -6$ eV was used. The resultant EXAFS data were weighted by k^3 $\{k = [2m(E - E_0)^{1/2}]/\hbar^2\}$ and Fourier transformed over the region of k = 1–14 Å. Least-squares fits of the EXAFS data were performed on Fourier-filtered EXAFS data, using the following formula to optimize the structural parameters N_b, R_{ab} and σ^2_{ab}:

$$\chi(k) = S_0^2(k) \sum_b \left(N_b/kR_{ab}^2\right) \left|f_b(k)\right| \exp\left(-2\sigma_{ab}^2 k^2\right) \times \exp\left[-2R_{ab}/\lambda(k)\right] \sin\left[2kR_{ab} + \varphi_{ab}(k)\right]. \quad (1)$$

In this equation, N_b is the number of backscatterers in the bth backscattering shell at distance R_{ab} from the X-ray absorber (Ni), $f_b(k)$ and $\varphi_{ab}(k)$ are the backscattering amplitude and total phase-shift of the absorber–scatterer pairs, σ^2_{ab} is the mean square deviation of R_{ab}, and $\lambda(k)$ represents the mean free path of the ejected photoelectron. $S_0^2(k)$ is an amplitude reduction factor that accounts for multiple electron excitations. MS paths were calculated with *FEFF* 7.0.1. The path contribution of less than 1% was rejected to reduce the free parameters in the EXAFS fitting process. Therefore only MS paths A, B and C were considered in our MS analysis (see Fig. 2). The goodness of the SS and MS fits was determined by $F = \Sigma(\chi_{calc} - \chi_{obs})^2 k^6$.

3. Results and discussion

3.1. *K*-edge XANES

The *K*-edge XANES spectra for **1** (green), **2** (blue) and **3** (red) were reported in a recent publication (Gu *et al.*, 2014). The *K*-edge position shifts +0.7 eV per oxidation state increase (or +0.7 eV/oxi) (see Table 1). This shift is also similar to that reported for $[Ni(MNT)_2]^{2-}$ *versus* $[Ni(MNT)_2]^{1-}$ (Eidsness *et al.*, 1988) (*ca* 1 eV/oxi). However, it is far smaller than the shift seen in Ni oxides (Mansour & Melendres, 1998), which is ∼1.85 eV/oxi (Mansour & Melendres, 1998; Gu *et al.*, 2014). This is consistent with the 'non-innocent' nature of the dithiolene ligands. Interestingly, *D. gigas* NiFe hydrogenase has a Ni *K*-edge shift of ∼1 eV between oxidized and reduced states (Davison & Holm, 1967; Gu *et al.*, 2003). This similarity supports the biological relevance of these dithiolene complexes.

Table 1
K-edge positions, shifts and pre-edge feature observations for complexes **1**, **2**, **3** and **4**.

	Complex **1**	Complex **2**	Complex **3**	Complex **4**
K-edge, E_i (eV)	8339.1	8339.8	8340.5	8339.7
E_i shift (eV)	0.0	+0.7	+1.4	+0.6
Pre-edge features	Yes	Yes	Yes	No

The XANES spectra for the 1-hexene adduct **4** (purple) and for its parent dithiolene complex **3** are shown in Fig. 3. There is an intense peak in the 8336–8338 eV region for **3** (red), which is due to a $1s \rightarrow 4p_z$ transition, a typical XANES feature for square planar complexes (Bagyinka *et al.*, 1993; Gu *et al.*, 2014). The XANES for **1**, **2** and **3** have been published (Gu *et al.*, 2014) and all of them have a $1s \rightarrow 4p_z$ peak. The *K*-edge XANES for the 1-hexene adduct $Ni[S_2C_2(CF_3)_2]_2(C_6H_{12})$ (**4**), on the other hand, shows no $1s \rightarrow 4p_z$ peak or any other peak in the transition region (Fig. 3). The lack of pre-edge peak in XANES is consistent with the fact that adding 1-hexene across the ligand sulfur atoms breaks the square planar symmetry in **3** (Fig. 1, **A**), as suggested by the change in the HOMO → LUMO transition (744 nm) seen in UV/visible spectroscopy (Wang & Stiefel, 2001). Although the crystal structure for **4** is not available, the crystal structure for a similar olefin adduct, $Ni[S_2C_2(CF_3)_2]_2(C_2H_4)$, has been reported (Harrison *et al.*, 2006). A bowl-type distortion was shown, similar to that in the norbornadiene (NBD) adduct, $Ni[S_2C_2(CF_3)_2]_2$(NBD) (Wing & Schlupp, 1970). The C_2H_4 bridge is twisted with a 19.7° torsion, leading to *C*1 molecular symmetry.

The *K*-edge energy position for **4** is 0.8 eV lower than that for **3** (0.6 *versus* 1.4 eV in reference to **1**). These observations

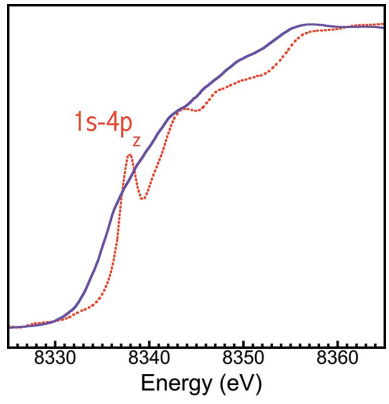

Figure 3
Ni *K*-edge XANES spectra in the 8325–8365 eV region for **3** (dashed red) and the 1-hexene adduct **4** (solid purple). The pre-edge feature for **3** disappears after the 1-hexene adduction.

indicate that the neutral complex is 'reduced' upon addition of olefin, presumably by olefin donating the π-electron density to the LUMO of **3** as suggested by the change in UV/visible spectroscopy in the literature (Wang & Stiefel, 2001).

3.2. EXAFS spectra

After spline removal, the unfiltered and k^3-weighted EXAFS $\chi(k)$ spectra for **1**, **2**, **3** and **4** are shown in Fig. 4 (left panel). The spectra for **1**, **2** and **3** appear very similar. However, careful comparison reveals subtle differences in their EXAFS oscillation frequency. According to a simple EXAFS theory, the shorter the bond length, the higher the EXAFS oscillation frequency (Agarwal, 1991; Penner-Hahn, 1999). This gives us an indication that the Ni—S distances are different for different complexes. The oscillation frequency and pattern for the olefin adduct **4** is significantly different from **1**, **2**, **3**; and its oscillation amplitude becomes much smaller as well, indicating a significantly distorted structure for **4** (Penner-Hahn, 1999).

The Fourier transformation (FT) of the phase-uncorrected (above) EXAFS for **1**, **2**, **3** and **4** are presented in Fig. 4 (right-hand panel, colored solid lines). The main peaks in these spectra are all centered at *ca* 1.7 Å (a phase-uncorrected value), which corresponds to the interactions between Ni and the first shell scatterers (S). Single-scattering simulation of these data found that the (phase-corrected) Ni—S coordination distances are at 2.159 Å, 2.134 Å and 2.115 Å for compounds **1**, **2** and **3**, respectively, which fall in the range for typical four-coordinated square planar Ni complexes (from 2.10 Å to 2.24 Å) (Churchill *et al.*, 1971). Among **1**, **2** and **3**, the Ni—S bond length decreases by about 0.022 Å as the complex is formally oxidized by one electron. Similar trends (*ca* 0.02 Å/oxi) were observed in other Ni dithiolene compounds such as $[Ni(S_2C_2Ph_2)_2]^{0,1-}$ (Mahadevan *et al.*, 1984; Megnamisi-Belombe & Nuber, 1989; Sartain & Truter, 1967) and $[Ni(S_2C_2Me_2)_2]^{0,1-,2-}$ (Lim *et al.*, 2001). The trend is also consistent with the X-ray crystal structural for **2** and **3** (the Ni—S distances decrease by 0.011 Å/oxi) (Wang *et al.*, 2007). However, the change here is much less than the changes in the Ni—O distances in nickel oxides, which is ~0.1 Å (Mansour & Melendres, 1998). This is not surprising because Ni dithiolenes have non-innocent ligands; one-electron redox of the complexes does not result in the change of nickel oxidation state by one unit (Gu *et al.*, 2014).

The average Ni—S distance for **4** is 2.155 Å, consistent with those in the ethylene adduct [2.159–2.163 Å (Harrison *et al.*, 2006)]. Although the edge position of **4** is close to that of **2**, the Ni—S distance is close to that of **1**. The further elongation of the Ni—S distance in **4** is consistent with the distorted bowl-shaped structure for the olefin adduct (Harrison *et al.*, 2006). We also noted that the Debye–Waller factor (σ) for the Ni—S interactions is much higher for **4** ($\sigma^2 = 5.2 \times 10^{-3}$ Å^2) than those for **1**, **2**, **3** (2.2–2.7 $\times 10^{-3}$ Å^2) (Table 2). A higher

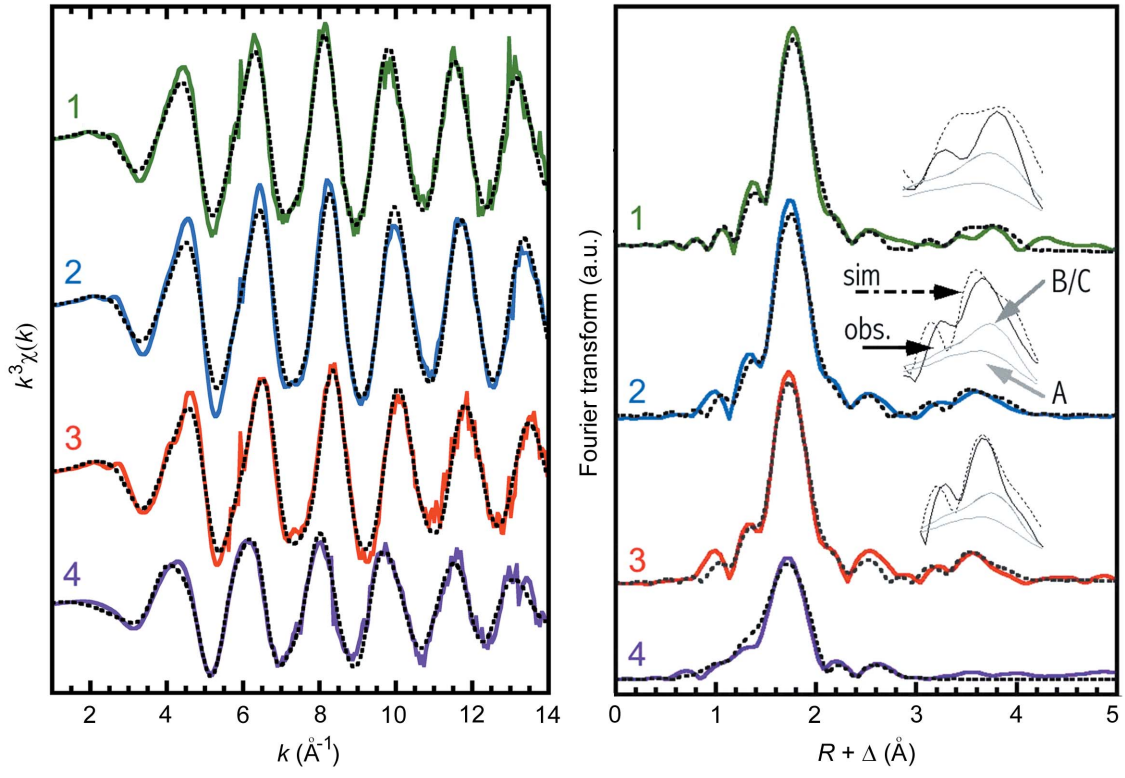

Figure 4
Left-hand panel: the observed (solid colored lines) and MS fitted (dashed black lines) EXAFS *k*-space spectra for **1** (green), **2** (blue), **3** (red) and **4** (purple). Right-hand panel: Fourier-transformed (FT) experimental EXAFS (solid colored lines) and the best MS fits (dashed black lines) for **1** (green), **2** (blue), **3** (red) and **4** (purple). Insets in the right-hand panel: the magnified long-distance FT peaks in the experimental EXAFS (top solid lines) and in the best MS fits (top dashed lines). The curves underneath them correspond to the contributions from the MS scattering paths of A (lower) and MS B or C (middle).

Table 2
Single-scattering fit parameters for Ni dithiolene complexes **1**, **2**, **3** and **4**.

Complexes	*N*	*R* (Å)	σ^2 (10^{-3} Å^2)	Φ
1	4S	2.159	2.70	398.3
	4C	3.104	4.28	
2	4S	2.134	2.24	350.4
	4C	3.067	5.62	
3	4S	2.115	2.22	344.6
	4C	3.041	5.59	
4	4S	2.155	5.22	159.8
	4C	3.090	5.43	

Debye–Waller factor (σ) indicates a more disordered (S) shell, which can be induced by asymmetric addition of 1-hexene to the S ligands (see Fig. 1), again consistent with the crystal structures for the olefin adducts (Harrison *et al.*, 2006).

Adding one more shell of C (see Fig. 4) improves the simulation by fitting the second peak at *ca* 2.5 Å (phase-uncorrected spectra, Fig. 5). The analyzed (phase-corrected) Ni—C distances for **1**, **2** and **3** are at 3.106 Å, 3.067 Å and 3.041 Å, respectively, and that for **4** is at 3.090 Å, as summarized in Table 2.

4. MS analysis

There are weak contributions at *ca* 3.2 Å and 3.5 Å (Fig. 5), which cannot be reproduced *via* SS simulation. MS calculations are thus necessary in order to fit these 'minor' peaks. The *FEFF* (Rehr *et al.*, 1991) calculation for **1**, **2** and **3** yields two single SS paths, which correspond to Ni—S and Ni—C, and seven MS paths as illustrated in detail in Fig. 2. Among the MS paths, paths A, B and C correspond to the three- and four-legged paths in the linear arrangement of S—Ni—S. The others are the non-linear three- and four-legged paths involving C or S or both shells. The individual EXAFS contribution of each path used in the fit is shown in Fig. 5, using complex **1** as an example. Ni—S contributes ~77.5% of the overall EXAFS intensity (scaled by 50% in Fig. 5 for a better illustration of other contributions); Ni—C contributes ~7.3%; while MS A/B/C contribute 3.1%/6.0%/6.0%. Other MS have less than 0.1% contribution, and are thus omitted. MS contributes about 15.1% to the overall EXAFS oscillations.

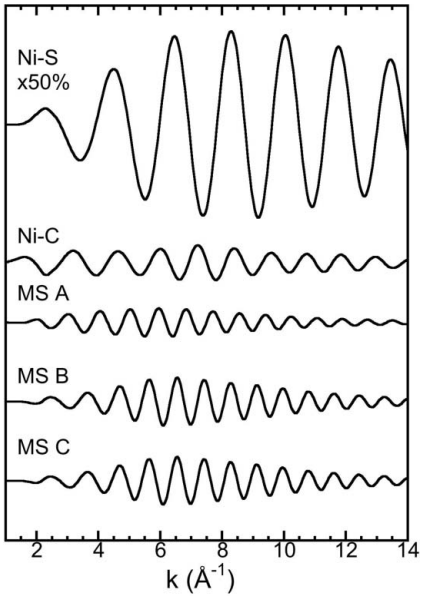

Figure 5
Various SS and MS EXAFS scattering contributions for complexes **1**: Ni—S (77.5%, curve scaled by 50%); Ni—C (7.3%); MS A (3.1%); MS B (6.0%) and MS C (6.0%). For SS and MS scattering paths, refer to Fig. 2 and the text for details.

Table 3
Multiple-scattering fit parameters for Ni dithiolene complexes **1**, **2** and **3**.

Complexes	*N*	*R* (Å)	σ^2 (10^{-3}Å^2)	Φ
1	4S	2.159	2.70	334.9
	4C	3.104	4.28	
	4 Path A	4.318	2.56	
	4 Path B	4.318	2.56	
	4 Path C	4.320	2.56	
2	4S	2.134	2.24	298.0
	4C	3.067	5.62	
	4 Path A	4.267	3.36	
	4 Path B	4.267	3.36	
	4 Path C	4.269	3.36	
3	4S	2.115	2.22	303.5
	4C	3.041	5.59	
	4 Path A	4.231	3.34	
	4 Path B	4.231	3.34	
	4 Path C	4.233	3.34	

The best MS simulations of the dithiolene complexes **1**, **2**, **3** are shown in Fig. 4 (left-hand and right-hand panels, dashed lines for **1**, **2**, **3**). Although the MS contributions are minor compared with the Ni—S shell, the peaks at distances of 3.2 and 3.5 Å (phase-uncorrected spectra) can only be fitted when MS simulations are included. The MS path lengths obtained from the MS simulation agree well with the SS analysis. For example, the S—Ni—S path length is exactly twice the value for the Ni—S distance (Tables 2 and 3). It should also be noticed that MS B and MS C (the middle grey curves in the insets of Fig. 4, right-hand panel) are identical due to the complexes' square planar symmetry. This 'degeneracy' also explains that only two MS curves (one for A and one for B/C) are shown in Fig. 4 (right-hand panel). For the olefin adduct product **4**, there are no peaks in the MS region (Fig. 4, right panel, purple curve). This seems reasonable because MS contributions are obvious only for a symmetric structure around the scattering (Ni) atom, while **4** has a *C*1 symmetry (Harrison *et al.*, 2006).

Metal–metal bonding is of great interest in bio-inorganic chemistry, especially for some metalloenzymes in the reduced states, where it stabilizes low-valent metal centers poised for substrate activation. For example, Ni—Fe interactions are proposed for Ni–L NiFe hydrogenase (Kampa *et al.*, 2013) and for carbon monoxide dehydrogenase (CODH) (Jeoung & Dobbek, 2009), Ni—Ni and Fe—Fe bonding are proposed for acetyl-CoA synthetase (Lindahl, 2012) and [FeFe]-H_2ase (Nicolet *et al.*, 2001). While these metal–metal interactions are typically in the range of ~3 Å, metal–C interactions and MS parameters are also at ~3 Å, complicating EXAFS studies on these important metal–metal interactions [by the existence of metal–C/metal–N interactions as well as MS scattering effects

(Riggs-Gelasco *et al.*, 1995)]. The work we report here illustrates the power of MS EXAFS in elucidating the structures of dithiolene complexes as a result of better EXAFS fitting. This approach could also potentially be used to evaluate the influence of the above-mentioned 'side effect' (metal–C and MS) while probing the metal–metal interactions in bioinorganic EXAFS.

This publication also shows that, although undulator beamlines are more advanced today, bent-magnet-based beamlines are still useful for resolving ambiguous chemical issues.

5. Summary

A series of Ni dithiolene complexes $Ni[S_2C_2(CF_3)]_2^n$ ($n = -2$, -1, 0) (**1**, **2**, **3**), and a 1-hexene adduct $Ni[S_2C_2(CF_3)_2]_2(C_6H_{12})$ (**4**) have been examined by Ni *K*-edge XANES and EXAFS. Ni XANES for **1**–**3** reveals clear pre-edge features and the *K*-edge position shifts approximately +0.7 eV for one-electron oxidation in the complexes. EXAFS fits show that: (i) the Ni—S bond distances for **1**, **2** and **3** (2.11–2.16 Å) are typical for square planar complexes; (ii) the bond distance decreases by ~0.022 Å for each one-electron oxidation; (iii) the Ni—C interactions are at 3.106 Å, 3.067 Å and 3.041 Å; (iv) MS simulation provided a much better EXAFS fit for symmetric structures, such as **1**, **2** and **3**. The trends in energy positions and Ni—S distances are both consistent with the 'non-innocent' character of the dithiolene ligand.

The first XANES and EXAFS studies for a nickel dithiolene–olefin adduct **4** are also reported here. The spectra are different from those for **1**, **2** and **3**. In the XANES region, **4** presents no pre-edge feature and its Ni *K*-edge position shifts by −0.8 eV in comparison with its starting dithiolene complex **3**, consistent with the value for one-electron reduction. EXAFS showed that the Ni—S distances in **4** elongate ~0.046 Å in comparison with **3**, close to two-electron reduction. Although the exact change in the oxidation state of nickel in the dithiolene complex upon olefin addition is not quantitatively clear, the evidence confirms that the neutral complex is 'reduced' upon addition of olefin, presumably by olefin donating the π-electron density to the LUMO of **3** as suggested by UV/visible spectroscopic data in the literature (Wang & Stiefel, 2001). A combination of theoretical (Fan & Hall, 2002) and experimental (UV/visible spectroscopy, X-ray absorption spectroscopy and crystal structure determination, *etc.*) studies, employing olefins with different electron density in the π-orbital, should help to further understand the impact of the nature of the olefin on the oxidation state of nickel in the olefin adduct.

References

Agarwal, B. K. (1991). *X-ray Spectroscopy: An Introduction*, 2nd ed. New York: Springer-Verlag.

Bagyinka, C., Whitehead, J. P. & Maroney, M. J. (1993). *J. Am. Chem. Soc.* **115**, 3576–3585.

Billig, E., Williams, R., Bernal, I., Waters, J. H. & Gray, H. B. (1964). *Inorg. Chem.* **3**, 663–666.

Chen, C. T., Liao, S. Y., Lin, K. J. & Lai, L. L. (1998). *Adv. Mater.* **10**, 334–338.

Churchill, M. R., Cooke, J., Fennessey, J. P. & Wormald, J. (1971). *Inorg. Chem.* **10**, 1031–1035.

Davison, A. & Holm, R. H. (1967). *Inorg. Synth.* **10**, 8–26.

Eidsness, M. K., Sullivan, R. J. & Scott, R. J. (1988). *The Bioinorganic Chemistry of Nickel*, edited by J. R. Lancaster Jr, pp. 73–91. New York: VCH.

Fan, Y. & Hall, M. B. (2002). *J. Am. Chem. Soc.* **124**, 12076–12077.

George, G. G. (2009). *EXAFSPAK*, http://xafs.org/Software/EXAFSPAK.

Gray, H. B. (1965). *Transit. Metal Chem.* **1**, 239–287.

Gu, W. W., Jacquamet, L., Patil, D. S., Wang, H. X., Evans, D. J., Smith, M. C., Millar, M., Koch, S., Eichhorn, D. M., Latimer, M. & Cramer, S. P. (2003). *J. Inorg. Biochem.* **93**, 41–51.

Gu, W., Wang, H. & Wang, K. (2014). *Dalton Trans.* **43**, 6406–6413.

Harrison, D. J., Nguyen, N., Lough, A. J. & Fekl, U. (2006). *J. Am. Chem. Soc.* **128**, 11026–11027.

Jeoung, J.-H. & Dobbek, H. (2009). *J. Am. Chem. Soc.* **131**, 9922–9923.

Kampa, M., Pandelia, M.-E., Lubitz, W., van Gastel, M. & Neese, F. (2013). *J. Am. Chem. Soc.* **135**, 3915–3925.

Lim, B. S., Fomitchev, D. V. & Holm, R. H. (2001). *Inorg. Chem.* **40**, 4257–4262.

Lindahl, P. A. (2012). *J. Inorg. Biochem.* **106**, 172–178.

McCleverty, J. A. (1968). *Prog. Inorg. Chem.* **10**, 49–221.

Mahadevan, C., Seshasayee, M., Kuppusamy, P. & Manoharan, P. T. (1984). *J. Crystallogr. Spectrosc. Res.* **14**, 179–191.

Mansour, A. N. & Melendres, C. A. (1998). *J. Phys. Chem. A*, **102**, 65–81.

Megnamisi-Belombe, M. & Nuber, B. (1989). *Bull. Chem. Soc. Jpn*, **62**, 4092–4094.

Mueller-Westerhoff, U. T., Vance, B. & Yoon, D. I. (1991). *Tetrahedron*, **47**, 909–932.

Nicolet, Y., de Lacey, A. L., Vernède, X., Fernandez, V. M., Hatchikian, E. C. & Fontecilla-Camps, J. C. (2001). *J. Am. Chem. Soc.* **123**, 1596–1601.

Olson, D. C., Mayweg, V. & Schrauzer, G. N. (1966). *J. Am. Chem. Soc.* **88**, 4876–4882.

Paw, W., Cummings, S. D., Adnan Mansour, M., Connick, W. B., Geiger, D. K. & Eisenberg, R. (1998). *Coord. Chem. Rev.* **171**, 125–150.

Penner-Hahn, J. E. (1999). *Coord. Chem. Rev.* **190–192**, 1101–1123.

Reedijk, J. & Bouwman, E. (1999). *Bioinorganic Catalysis.* New York: Marcel Dekker.

Rehr, J. J., Mustre De Leon, J., Zabinsky, S. I. & Albers, R. C. (1991). *J. Am. Chem. Soc.* **113**, 5135–5140.

Riggs-Gelasco, P. J., Stemmler, T. L. & Penner-Hahn, J. E. (1995). *Coord. Chem. Rev.* **144**, 245–286.

Sartain, D. & Truter, M. R. (1967). *J. Chem. Soc. A*, pp. 1264–1272.

Schrauzer, G. N. (1969). *Acc. Chem. Res.* **2**, 72–80.

Schrauzer, G. N. & Mayweg, V. P. (1965). *J. Am. Chem. Soc.* **87**, 1483–1489.

Wang, H. X., Ralston, C. Y., Patil, D. S., Jones, R. M., Gu, W., Verhagen, M., Adams, M., Ge, P., Riordan, C., Marganian, C. A., Mascharak, P., Kovacs, J., Miller, C. G., Collins, T. J., Brooker, S., Croucher, P. D., Wang, K., Stiefel, E. I. & Cramer, S. P. (2000). *J. Am. Chem. Soc.* **122**, 10544–10552.

Wang, K., Patil, A. O., Zushma, S. & McConnachie, J. M. (2007). *J. Inorg. Biochem.* **101**, 1883–1890.

Wang, K. & Stiefel, E. I. (2001). *Science*, **291**, 106–109.

Westre, T. E., Kennepohl, P., DeWitt, J. G., Hedman, B., Hodgson, K. O. & Solomon, E. I. (1997). *J. Am. Chem. Soc.* **119**, 6297–6314.

Wing, R. M. & Schlupp, R. L. (1970). *Inorg. Chem.* **9**, 471–475.

Winter, C. S., Oliver, S. N., Rush, J. D., Hill, C. A. S. & Underhill, A. E. (1992). *J. Appl. Phys.* **71**, 512–514.

Yadav, J., Das, S. K. & Sarkar, S. (1997). *J. Am. Chem. Soc.* **119**, 4315–4316.